

Effect of H-Atom on Local Structure in Ni–Zr–Nb Amorphous Alloy

N. FUJIMA^{a,*}, T. HOSHINO^a AND M. FUKUHARA^b

^aDepartment of Electronics and Material Science, Shizuoka University, Naka-ku Hamamatsu 432-8561, Japan

^bNew Industry Creation Hatchery Center, Tohoku University, Tagajyo 985-8589, Japan

We optimize the atomic structures of icosahedral $\text{Ni}_6\text{Zr}_5\text{Nb}_3$ with an added H-atom in a periodic cell as a local structural model of Ni–Zr–Nb–H amorphous alloys by the first principles calculation, and identify energetically favorable H-atom sites in the local structure of the amorphous alloys. We find that a H-atom is favorably located not at tetrahedral sites in the icosahedral cluster but at octahedral sites in the region of inter-cluster. We also find that a H-atom in some tetrahedral sites induces a rearrangement of the local structure from icosahedral to fcc-like, which seems to correspond to a local crystallization in the amorphous phase. These results give a fundamental behavior of hydrogen atoms in Ni–Zr–Nb amorphous alloys and information to elucidate the mechanism of the electrical transport in the Ni–Zr–Nb amorphous alloys with H-atoms.

DOI: [10.12693/APhysPolA.128.709](https://doi.org/10.12693/APhysPolA.128.709)

PACS: 61.43.Dq, 61.43.Bn, 71.23.Cq, 71.15.Mb

1. Introduction

Nickel–zirconium amorphous and related alloys have been developed and studied because of the high storage ability and permeability to hydrogen. Not only various compositions of binary alloys [1], but also a huge number of ternary alloys, such as Ni–Zr–Al [2], Ni–Zr–Ti [3], and Ni–Zr–Nb [4], have been examined to improve the performance and stability of the systems. For example, Yamaura et al. reported that melt-spun Ni–Zr–Nb amorphous alloy, $\text{Ni}_{30}\text{Zr}_{50}\text{Nb}_{30}$ has the excellent hydrogen permeability [5]. The influence on mechanical properties of the alloys by hydrogen-charge also was investigated, as well [6]. Fukuhara et al. observed some new interesting phenomena in the Ni–Zr–Nb–H amorphous alloys besides the high hydrogen permeability. They have reported on the electrical transport behavior in $(\text{Ni}_{0.6}\text{Nb}_{0.4})_{1-x}\text{Zr}_x)_{100-y}\text{H}_y$ ($0.3 \leq x \leq 0.5$, $0 \leq y \leq 20$) amorphous alloys as a function of their hydrogen concentration [7]. These alloys have shown negative temperature-derivative of resistivity, superior (ballistic) conducting and superconducting transport, and electric current-induced voltage (Coulomb) oscillation [8]. These results show that the localization effect of hydrogen both outside and inside the clusters plays an important role in various electrical transport phenomena.

In their works, they have reported the local atomic structures around the individual elements in the Ni–Zr–Nb alloys, such as coordination numbers (CNs) and interatomic distances investigated by X-ray absorption fine structure (XAFS) analysis [9–11]. They also reported on the local structural change by introducing H-atoms, and

have suggested some candidates for H sites in the Ni–Zr–Nb alloys. The effect of hydrogen-charge on the electrical transport properties of Ni–Zr–Nb amorphous alloys with various compositions was reported, too [12].

These structure assessments give useful suggestions to construct local atomic model of the Ni–Zr–Nb alloys with H-atoms and to elucidate the mechanism of the interesting phenomena mentioned above in the alloys. However they are limited to the first atomic shell, and have a certain ambiguity or inconsistency. Therefore, we first have to extract the (typical) local structure in the Ni–Zr–Nb alloys with the target composition, second we have to identify H-occupied sites, and concurrently search the rearrangement of the local structure by introducing H-atoms.

In our previous works, we explored the atomic structures of isolated (free) $\text{Ni}_5\text{Zr}_5\text{Nb}_3$ clusters, which are stoichiometrically similar to the bulk alloys, from the viewpoints of energetics and the optimized structures by the first principles calculation, and selected a candidate of the local structural unit within the first atomic shell from more than fifty isomers [13]. The candidate cluster has a relatively-low free energy, maintains the icosahedral shape after the optimization, and therefore is expected to have a substantial activation energy against the crystallization. We also proposed the larger structural unit which is composed of the candidate clusters, and discussed the fully optimized structures [14]. In the following section, we briefly describe the icosahedral structures of the $\text{Ni}_5\text{Zr}_5\text{Nb}_3$ cluster in the periodic cells.

In this paper, we introduce a H-atom in the cell which consists of the $\text{Ni}_5\text{Zr}_5\text{Nb}_3$ cluster with a Ni atom, and fully optimize structures of the $\text{Ni}_6\text{Zr}_5\text{Nb}_3+\text{H}$ cell. We search the energetically favorable H-atom sites both in the inner region of cluster and in the region of inter-cluster. We also discuss the rearrangement of the local structure by introducing a H-atom. We show that

*corresponding author; e-mail:
fujima.nobuhisa@shizuoka.ac.jp

a H-atom is favorably located not at tetrahedral sites in the inner region of cluster, but at octahedral or vacant sites in the region of inter-cluster, and that a H-atom in some sites induces a certain change of the local structure from icosahedral to fcc-like.

2. Calculations

Total energy calculations and structural optimizations are performed with VASP5.3, a plane-wave based density functional calculation package [15]. We employ the projector augmented-potential (PAW) [16] for the core orbitals under the generalized gradient approximation (GGA: PBE [17]). Semicore states, $4s$ and $4p$ are treated as valence states for Zr and Nb. The cutoff energy for the plane wave basis is 293.235 eV (NORMAL precision in VASP).

As the local structure of Ni–Zr–Nb alloy, we employ the following 14-atom unit cell as shown in Fig. 1: an icosahedral cluster, $\text{Ni}_5\text{Zr}_5\text{Nb}_3$ [13] is located at a vertex of a rhombohedral unit cell with the face angle of $\cos^{-1}(1/3) = 70.53^\circ$. The icosahedron connects with six adjacent icosahedra along their 3-fold rotational axes. Then, there exist six octahedron bridges between the icosahedra (two triangle facets constitute the octahedron without glue atom). Two alignments of the icosahedron are selected: (a) a Nb-triangle faces a Ni-triangle of an adjacent cluster (along the a -axis) (Fig. 1a), and (b) the Nb-triangle faces the direction of the diagonal (d -axis) of the rhombohedral unit cell (Fig. 1b). A Ni atom is added to the vacant region at the center of the cell. The property and structure of the icosahedral $\text{Ni}_5\text{Zr}_5\text{Nb}_3$ cluster as the local structural unit have been described in Refs. [13, 14].

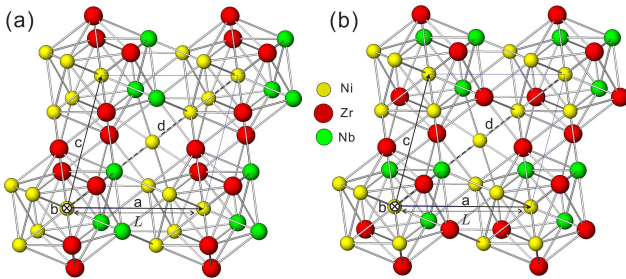


Fig. 1. Initial structures of the $\text{Ni}_6\text{Zr}_5\text{Nb}_3$ cell in two alignments: (a) Nb-triangle faces to a -axis, (b) Nb-triangle faces to diagonal (d)-line.

The atomic structures in Fig. 1a and b are fully optimized with varying the lattice parameter, L .

After the optimization of the cell, a H-atom is located at one of fourteen sites as the initial sites; three sites along each of the three edges (a -, b -, c -axes) and four sites along the d -axis in the optimized cell (see Fig. 2). Then the atomic structures of $\text{Ni}_6\text{Zr}_5\text{Nb}_3+\text{H}$ are fully optimized for each H-site to search the energetically favorable H-atom sites and the structural change by introducing a H-atom.

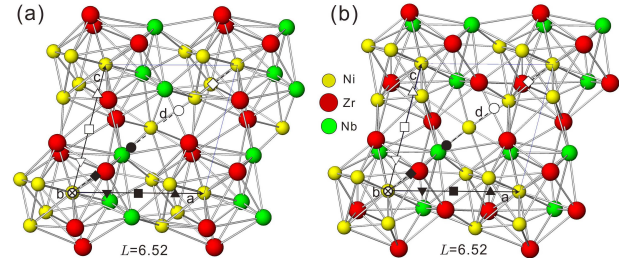


Fig. 2. Optimized structures of the $\text{Ni}_6\text{Zr}_5\text{Nb}_3$ cell at the equilibrium lattice parameter for the alignments (a) and (b). Symbols indicate the initial positions of a H-atom inserted.

3. Results and discussion

3.1. Optimized structures of $\text{Ni}_6\text{Zr}_5\text{Nb}_3$

Figure 3 shows total energies for the optimized structures of the $\text{Ni}_6\text{Zr}_5\text{Nb}_3$ cell around the equilibrium lattice parameter; open circles for the alignment (a) and filled circles for the alignment (b). The equilibrium cell length is $L = 6.52 \text{ \AA}$ while a small dip exists at $L = 6.57 \text{ \AA}$ for both the alignments. The total energy for alignment (b) is uniformly lower by 0.4 eV than that for alignment (a) within this region of the lattice parameter. This energy difference is mainly caused by the difference of Nb–Ni CN (number of Ni atoms surrounding a Nb atom) between the two alignments. We have revealed that the total energy of the isolated icosahedral Ni–Zr–Nb cluster linearly depends on the Nb–Ni CN [14].

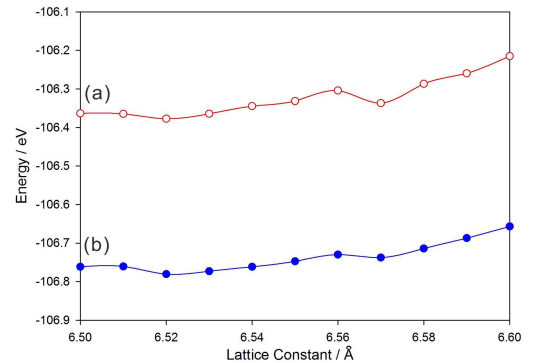


Fig. 3. Total energies of the $\text{Ni}_6\text{Zr}_5\text{Nb}_3$ cell in the optimized structures around the equilibrium lattice constant; open circles for the alignment (a), filled circle for the alignment (b).

The optimized structures at the equilibrium lattice parameter are shown in Fig. 2. The icosahedral shape of the cluster is well kept after the optimization for both alignments. The Voronoi index of the polyhedron around the Ni atom at the vertex of the cell is (0,0,12,0); 0, 0 for trigon, tetragon, 12 for pentagon and 0 for higher polygons. The optimized structures at other lattice parameters are similar to those in Fig. 2 although not shown here.

Symbols in Fig. 2 indicate the initial positions of an added H-atom described in the following subsection.

3.2. Optimized structures of $\text{Ni}_6\text{Zr}_5\text{Nb}_3+\text{H}$

Figure 4 shows the total energies of the optimized structures of $\text{Ni}_6\text{Zr}_5\text{Nb}_3+\text{H}$ around the equilibrium lattice parameter for the alignments (a) and (b). In the figure, black inverted triangles (\blacktriangledown), squares (\blacksquare), and triangles (\blacktriangle) indicate total energies for the initial H-atom positions along the a -axis with distances of 0.25 (\blacktriangledown), 0.5 (\blacksquare), and 0.75 (\blacktriangle) of the lattice parameter. The positions with the ratios of 0.25 and 0.75 correspond to the tetrahedral sites in the icosahedron and that with the ratio of 0.5 to the octahedral site in the bridge (see Fig. 2). Gray symbols (∇ , \square , \triangle) and open symbols (∇ , \square , \triangle) indicate those along the b - and c -axes, respectively. Diamonds and circles (\blacklozenge , \bullet , \circ , \diamond) indicate those along the diagonal (d -) axis (of the unit cell) with distances of 0.15 (\blacklozenge), 0.35 (\bullet), 0.65 (\circ), and 0.85 (\diamond) of the length of the diagonal line. The positions with the ratios of 0.15 and 0.85 correspond to the tetrahedral sites in the icosahedron, and those with the ratios of 0.35 and 0.65 to sites in the vacant area around the center of the cell. For the alignment (b) in Fig. 4b, the obtained energies for the H sites along the b -axis are almost the same as those along the c -axis because both the axes are symmetrically identical. Thus, the gray symbols for the former case are almost hidden by those for the latter case.

Abrupt energy-drops are observed around $L = 6.52$ and 6.57 \AA for the alignment (a) in Fig. 4a. These energy-drops suggest a singular structural change by introducing a H-atom. For example, the energy with a H-atom at the b -0.75 sites (\blacktriangle) falls down by about 2.5 eV from $L = 6.56$ to 6.57 \AA (indicated by double triangles in Fig. 4a). Figure 5 shows the optimized structures of the $\text{Ni}_6\text{Zr}_5\text{Nb}_3$ with a H-atom at the b -0.75 around this falling point, (a) at $L = 6.56 \text{ \AA}$ and (b) at $L = 6.57 \text{ \AA}$. Figure 5a indicates that the icosahedral structure similar to those in Fig. 2 still keeps after introducing a H-atom. The H-atom is located in the tetrahedron that consists of two Ni and two Zr atoms. On the other hand, Fig. 5b at $L = 6.57 \text{ \AA}$ shows an fcc-like distorted cuboctahedron with the Voronoi index (0,4,4,4) around the Ni atom at the vertex, in which the H-atom is located in a distorted square pyramid (one-half of octahedron that has changed from the tetrahedron). This structural change seems to correspond to a local crystallization, in which energetically higher amorphous states fall down to other energetically stable ordered states. A similar structural change has been observed in the optimized structure for a larger system, $\text{Ni}_{48}\text{Zr}_{40}\text{Nb}_{24}$ without introducing H-atoms [14].

On the contrary, the tendency of the energy curves in Fig. 4b (for the alignment (b)) is similar to those without H-atom in Fig. 3, so that the structure of the cell is little-affected by the added H-atom. All the optimized structures of $\text{Ni}_6\text{Zr}_5\text{Nb}_3+\text{H}$ for the alignment (b) keep the icosahedral shapes similar to that in Fig. 2b after adding a H-atom.

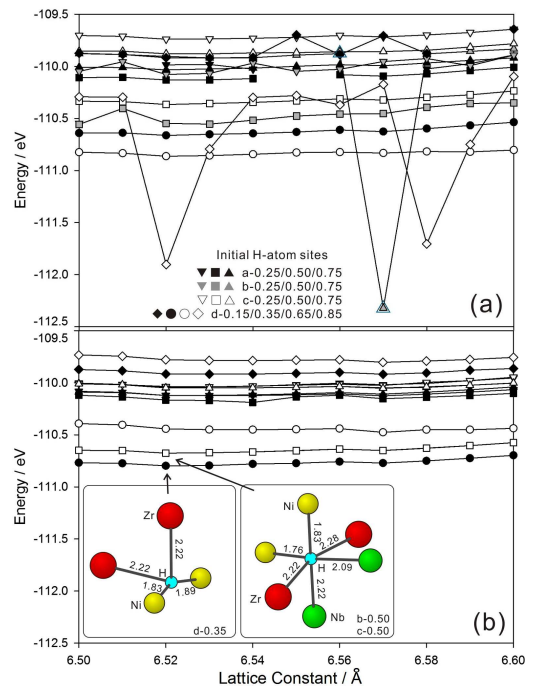


Fig. 4. Total energies in the optimized structures of the $\text{Ni}_6\text{Zr}_5\text{Nb}_3$ cell with a H-atom at the various initial sites for the alignments (a) and (b). Insets in (b) show the positions of atoms surrounding the H-atom with their interatomic distances in Å for the H-sites, d -0.35 and b/c -0.05 at $L = 6.52 \text{ \AA}$.

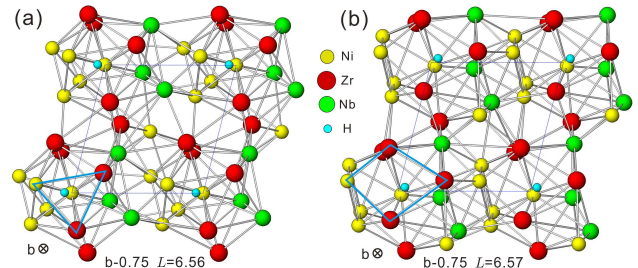


Fig. 5. Abrupt structural change in the optimized structure of the $\text{Ni}_6\text{Zr}_5\text{Nb}_3$ cell for the alignment (a) with a H-atom at b -0.75 site; (a) $L = 6.56 \text{ \AA}$ and (b) $L = 6.57 \text{ \AA}$.

The alignment (b) has a lower free energy than the alignment (a), and is expected to have a higher activation energy against the crystallization. Therefore, an added H-atom at some special sites does change the structure for the alignment (a), but does not change the structure for the alignment (b).

3.3. Position of H-atom in $\text{Ni}_6\text{Zr}_5\text{Nb}_3$

Figure 4 also suggests energetically favorable sites for H-atoms. All the energies with the H-atoms at the tetrahedral sites (indicated by symbols \blacktriangledown , \blacksquare , \blacktriangle etc. except for those around $L = 6.52$ and 6.57 \AA in the alignment (a) where the structural change occurs) constitute

the upper-side group in the figure while those at the vacant sites (\bullet , \circ) and the octahedral sites (indicated by \square etc.) constitute the lower-side group. Therefore the tetrahedral sites in the icosahedron are energetically unfavorable for a H-atom.

The H-atom sites for d -0.35 and c -0.50 (b -0.50) indicated by symbols \bullet and \square in Fig. 4b have the lowest energies in the alignment (b). Insets in Fig. 4b depict the atoms surrounding the H-atom with their interatomic distances in these lowest cases. The H-atom is surrounded by a one-quarter of octahedron, two Ni and two Zr atoms for d -0.35 (the left-hand inset), and by an octahedron, two Ni, two Zr, and two Nb atoms for c -0.50 (the right-hand inset). The interatomic distances of Ni–H (1.76–1.89 Å) in the insets are interestingly coincident with those in Ni-hydrates, NiH and Ni₂H (1.82–1.87 Å). These Ni–H distances suggest why a site in a Ni-tetrahedron is energetically unfavorable for a H-atom. A H-atom in a Ni-tetrahedron has too short Ni–H distances, and is expected to elongate the Ni–interatomic distance, hence, to rearrange the local atomic structure around the H-atom.

Recent vacancy analysis using positron annihilation spectroscopy and proton nuclear magnetic resonance studies suggested the existence of hydrogen atoms between Ni atoms that belong to different clusters [18, 19], as indicated in the insets in Fig. 4b.

3.4. Radial distribution functions of Ni atom in $Zr_5Ni_6Nb_3$

Figure 6 shows radial distribution functions (RDFs) $g_{Ni}(r)$ ($r = 2\text{--}4$ Å) around a Ni atom for the alignment (a); (a) the icosahedral structure at $L = 6.52$ Å without H-atom in Fig. 3a, and (b) the fcc-like structure with a H-atom along the b -axis (b -0.75) at $L = 6.57$ Å in Fig. 5a. There exist three peaks in the region of the first atomic shell (2.3–3.3 Å). The height of the main peak around 2.6 Å decreases while those of the side peaks increase when the atomic structure changes from icosahedral in Fig. 6a to cuboctahedral in Fig. 6b. The change in X-ray absorption fine structure (XAFS) profile (Ni K -edge) by introducing H-atoms [9, 11] seems to correspond to that in Fig. 6 although the XAFS profile cannot be compared directly with the RDFs because of the phase-shift of photoelectron wave in XAFS.

4. Summary

We optimize the atomic structures of icosahedral Ni₆Zr₅Nb₃ with an added H-atom in a periodic cell as a local structural model of Ni–Zr–Nb–H amorphous alloys by the first principles calculation, and identify energetically favorable H-atom sites in the local structure of the amorphous alloys. We find that a H-atom is favorably located not at tetrahedral sites in the icosahedral cluster but at some octahedral sites in the region of intercluster. We also find that a H-atom in some tetrahedral sites induces a rearrangement of the local structure from

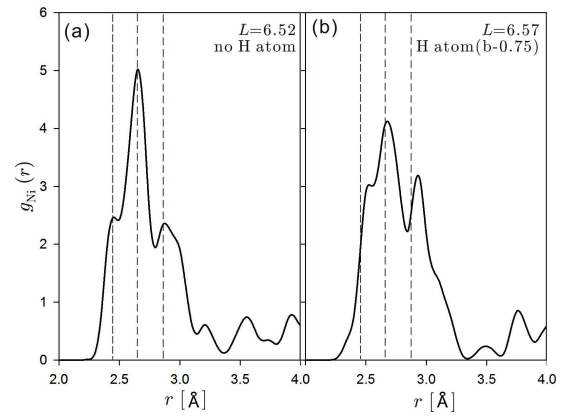


Fig. 6. Radial distribution functions for Ni atom in the Ni₆Zr₅Nb₃ cell: (a) for the icosahedral structure in Fig. 3a ($L = 6.52$ Å without H-atom), and (b) for the fcc-like structure in Fig. 5b ($L = 6.57$ Å with a H-atom at b -0.75 site).

icosahedral to fcc-like, which seems to correspond to a local crystallization in the amorphous phase. These results give a fundamental behavior of hydrogen atoms in Ni–Zr–Nb amorphous alloys and information to elucidate the mechanism of the interesting electrical transport in the Ni–Zr–Nb amorphous alloys with H-atoms.

References

- [1] Z. Altounian, T. Guo-hua, J.O. Strom-Olsen, *J. Appl. Phys.* **54**, 3111 (1983).
- [2] S. Sato, T. Sanada, J. Saida, M. Imafuku, E. Matsubara, A. Inoue, *Mater. Trans.* **46**, 2893 (2005).
- [3] A. Viano, E. Majzoub, R. Stroud, M. Kramer, S. Mixture, P. Gibbons, K. Kelton, *Philos. Mag. A* **78**, 131 (1998).
- [4] M. Sakurai, S. Yamamura, K. Wakoh, E. Matsubara, A. Inoue, *J. Metastable Nano. Mater.* **24**, 551 (2005).
- [5] S. Yamaura, Y. Shimpo, H. Okouchi, M. Nishida, O. Kajita, H. Kimura, A. Inoue, *Mater. Trans.* **44**, 1885 (2003).
- [6] A. Kawashima, S. Yamaura, N. Ohtsu, H. Kimura, A. Inoue, *Mater. Trans.* **47**, 1523 (2006).
- [7] M. Fukuhara, H. Yoshida, K. Koyama, A. Inoue, Y. Miura, *J. Appl. Phys.* **107**, 033703 (2010).
- [8] M. Fukuhara, M. Seto, A. Inoue, *Appl. Phys. Lett.* **96**, 043103 (2010).
- [9] H. Oji, K. Handa, J. Ide, T. Honma, S. Yamaura, A. Inoue, N. Umesaki, S. Emura, M. Fukuhara, *J. Appl. Phys.* **105**, 113527 (2009).
- [10] M. Fukuhara, N. Fujima, H. Oji, A. Inoue, S. Emura, *J. Alloys Comp.* **497**, 182 (2010).
- [11] M. Matsuura, M. Fukuhara, K. Konno, T. Fujita, M.W. Chen, N. Fujima, A. Inoue, *J. Non-Cryst. Solids* **375**, 3357 (2011).

- [12] R.Y. Umetsu, H. Yoshida, M. Fukuhara, S. Yamaura, M. Matsuura, T. Sasaki, T. Sekiguchi, M. Saito, J. Mizuno, H. Kawarada, *Mater. Trans.* **54**, 1339 (2013).
- [13] N. Fujima, K. Hara, T. Hoshino, M. Fukuhara, *Eur. Phys. J. D* **63**, 177 (2011).
- [14] N. Fujima, T. Hoshino, M. Fukuhara, *J. Appl. Phys.* **114**, 063501 (2013).
- [15] G. Kresse, J. Furthmüller, *Phys. Rev. B* **54**, 11169 (1996).
- [16] D. Vanderbilt, *Phys. Rev. B* **41**, 7892 (1990).
- [17] J.P. Perdew, A. Ruzsinszky, G.I. Csonka, O.A. Vydrov, G.E. Scuseria, L.A. Constantin, X. Zhou, K. Burke, *Phys. Rev. Lett.* **100**, 136406 (2008).
- [18] M. Fukuhara, *Appl. Phys. Lett.* **100**, 093102 (2012).
- [19] H. Niki, H. Okuda, M. Oshiro, M. Yogi, I. Seki, M. Fukuhara, *J. Appl. Phys.* **111**, 124308 (2012).